On the Use of Doppler Shift for Sea Surface Wind Retrieval From SAR

Alexis A. Mouche, Fabrice Collard, Bertrand Chapron, Knut-Frode Dagestad, Gilles Guitton,
Johnny A. Johannessen, Vincent Kerbaol, and Morten Wergeland Hansen

Abstract—The synthetic aperture radar (SAR) Doppler centroid has been used to estimate the scatter line-of-sight radar velocity. In weak to moderate ocean surface current environment, the SAR Doppler centroid is dominated by the directionality and strength of wave-induced ocean surface displacements. In this paper, we show how this sea state signature can be used to improve surface wind retrieval from SAR. Doppler shifts of C-band radar return signals from the ocean are thoroughly investigated by colocating wind measurements from the ASCAT scatterometer with Doppler centroid anomalies retrieved from Envisat ASAR. An empirical geophysical model function (CDOP) is derived, predicting Doppler shifts at both VV and HH polarization as function of wind speed, radar incidence angle, and wind direction with respect to radar look direction. This function is used into a Bayesian inversion scheme in combination with wind from *a priori* forecast model and the normalized radar cross section (NRCS). The benefit of Doppler for SAR wind retrieval is shown in complex meteorological situations such as atmospheric fronts or low pressure systems. Using *in situ* information, validation reveals that this method helps to improve the wind direction retrieval. Uncertainty of the calibration of Doppler shift from Envisat ASAR hampers the inversion scheme in cases where NRCS and model wind are accurate and in close agreement. The method is however very promising with respect of future SAR missions, in particular Sentinel-1, where the Doppler centroid anomaly will be more robustly retrieved.

Index Terms—Doppler, surface wind, synthetic aperture radar (SAR).

I. INTRODUCTION

WIND vectors over ocean are linked to the ocean roughness and the normalized radar cross section (NRCS) as detected by active radar sensors such as scatterometers or synthetic aperture radar (SAR).

Scatterometers provide daily global wind estimates which have made a unique and invaluable contribution to the continuously improving accuracy of weather forecast models over the last decades. The relatively coarse spatial resolution of scatterometers (order of 10 km) is still a limitation in coastal regions, where most human offshore activities are confined. Mesoscale variations of wind, often induced by topography effects, land-sea breezes, or convective structure, are usually not resolved, and strong radar backscatter from land inhibits wind retrieval closer than 15 km from the coast.

SAR systems, on the other hand, provide a spatial resolution of the order of tens of meters, to provide information even inside narrow bays and fjords [1]. However, a SAR is a single antenna instrument, while the relationship between wind and NRCS depends strongly on the radar look direction relative to the wind direction (e.g., [2]). Scatterometers use a rotating antenna, or several fixed antennas, to view a given area of the ocean from different directions, to help interpret the measured radar signal intensity in terms of wind speed and direction. For SAR, the wind inversion becomes an underconstrained problem. The simplest and most common solution is to estimate the wind by assuming the wind direction is known from a numerical weather prediction (NWP) model or scatterometry measurements close in time [3] and obtaining the high-resolution wind speed by the interpretation of the NRCS. This works generally well offshore, where gradients of wind directions are quite small, but is not always adequate in coastal regions where local effects are not properly resolved by the forecast models. Moreover, in cases of rapidly changing meteorological situations such as wind fronts or cyclones, a phase shift (in space and/or time) between prediction and actual situation often occurs, making this solution inadequate. Another resource is to retrieve the wind direction from image processing of visible streaks on the SAR image, caused by boundary layer rolls which are aligned with the wind direction [4], [5]. This is not always satisfactory. The streaks are indeed not always detectable, and nonwind related features may also give linear features on the image. On the top of that, wind directions deduced from streaks analysis and wind direction from NWP can be very different [6]. To overcome these difficulties, a scheme for an optimal retrieval of both wind components was suggested by [6] who introduced a statistical (Bayesian) method to combine the NRCS as measured by SAR with both wind speed and direction from a NWP model.

Recently, a new resource for SAR wind inversion has become available. [7] demonstrated how the Doppler centroid anomaly from ENVISAT ASAR could be used to retrieve geophysical information about both wind and sea surface current. Indeed, a residual Doppler comes from the line-of-sight motions of the surface scattering elements relative to the fixed earth. Only the component along the SAR look direction is detected. The

A. A. Mouche, F. Collard, and V. Kerbaol are with the Direction of Radar Applications, CLS, 29280 Plouzané, France (e-mail: amouche@cls.fr; fcollard@cls.fr; vkerbaol@cls.fr).

B. Chapron and G. Guitton are with CERSAT, IFREMER, 29280 Plouzané, France (e-mail: bchapron@ifremer.fr; gguitton@ifremer.fr).

K. F. Dagestad, J. A. Johannessen, and M. W. Hansen are with the Nansen Environmental and Remote Sensing Center, 5006 Bergen, Norway (e-mail: knut-frode.dagestad@nersc.no; johnny.johannessen@nersc.no; morten.hansen@nersc.no).

ocean surface current contributes to a degree which depends on the relative velocities of the wind and currents, as well as their directions relative to the SAR look direction. After [7], a jointly developed model to interpret both radar cross section and Doppler information has been reported by [9], and Doppler has been used to study strong surface current signatures [10]. This paper is the first study to focus on use of SAR Doppler centroid anomalies for wind retrieval.

In Section II, we discuss the wind signature in the Doppler shift with respect to the radar configuration and present an empirical function (CDOP) to relate wind intensity and direction to C-band Doppler shift. In Section III-A, we describe a method to take into account this Doppler information into a SAR wind retrieval scheme. In Section III-B, this method is demonstrated for two SAR images with complex wind conditions, followed by validation against *in situ* buoy measurements. Summary and further perspectives are given in Section IV.

II. WIND SIGNATURE IN THE SAR DOPPLER CENTROID ANOMALY

A. Doppler Shift From Envisat ASAR

The Doppler centroid has been regularly available in Envisat ASAR WSM products as an auxiliary data set since July 2007, following the demonstration by [7] that it contains useful geophysical information. It is available with a pixel spacing of about 8 km along the azimuth direction, and in the range direction varying from 8 km in near range to 3.5 km in far range. Details on Doppler centroid estimation algorithm are given in ASAR Handbook [8].

The dominant contribution to the Doppler centroid frequency is the relative velocity of the satellite and the surface of the rotating earth. This can be estimated using a geometric model and removed. The residual Doppler shift or Doppler anomaly, of interest here, reflects the radar detected motions relative to the fixed earth. However, even after geometric correction, two strong biases still mask the geophysical information in the Doppler anomaly and must first be corrected for.

One source of bias is caused by azimuthal variations of the NRCS within the Doppler resolution cell over which a single Doppler centroid is estimated. The part of the Doppler resolution cell which is ahead/behind (in the flight direction) of the zero Doppler line contributes positively/negatively to the Doppler Centroid estimate. These contributions are however weighted by the local NRCS, and hence any azimuthal variations of NRCS may lead to a bias of the Doppler centroid anomaly, independent of any surface motions. A postprocessing correction for this "azimuth bias" is to find an empirical average linear fit between the Doppler centroid values and the corresponding linear gradient of NRCS in the azimuth direction. For a given ASAR WSM scene, this mapping is then used to calculate a Doppler Centroid bias which is removed.

A second independent bias is due to the deviation of the actual azimuth antenna pattern from the theoretical antenna pattern used within the SAR processor. This leads to an electronical mispointing, which adds to the physical mispointing from imperfectly known satellite attitude parameters. Together, this causes an offset which varies strongly with the look angle (in the range direction), but varies slowly with time, and can be regarded as constant along azimuth for a standard SAR scene. A first order correction for this "range bias" is obtained by subtracting the average Doppler Centroid value for the portion of each azimuth line which is over land.

The details of calculating and calibrating the Doppler centroid anomaly, even when land coverage is not available, are given in [11]. An accuracy of the 5 Hz was found by [11], corresponding to a horizontal surface velocity change of 20 cm/s at an incidence angle of $40°$, and of 40 cm/s at an incidence angle of $20°$. The contribution to the Doppler shift from (wind induced) ocean waves is discussed in the next section.

B. Relationship Between Doppler Shift and Wind

To perform wind inversion from the normalized radar cross section, empirical geophysical model functions (GMFs) such as CMOD (e.g., [2], [12], or [13]) are normally used. Such functions relate the wind speed and direction (with respect to the antenna look direction) to the NRCS with respect to radar configuration (radar wavelength, polarization, and incidence angle). In this paper, we assess the variation of the Doppler shift as a function of wind and radar configurations, and a GMF for Doppler shift by colocating wind measurements at 10 m height from ECMWF (updated every 6 h with $0.5°$ spatial resolution) with C-band ASAR Doppler anomalies. We built a match-up database between wind speed and direction from ECMWF, collocated with incidence angle and Doppler measurements from ASAR leading to 277211 and 350007 colocations for VV and HH polarizations, respectively. Fig. 1(a) and (d) show the Doppler anomaly (squares) with respect to incidence angle ($±0.5°$) for a 7 m/s ($±2$ m/s) wind speed in upwind (wind blowing toward the antenna $±20°$) and downwind (wind blowing away from the antenna $±20°$) directions. Fig. 1(b) and (e) shows the Doppler anomaly (squares) with respect to wind speed ($±1$ m/s) for $40°$ ($±1°$) incidence angle in upwind ($±20°$) and downwind ($±20°$) directions. Fig. 1(c) and (f) show the Doppler anomaly (squares) with respect to azimuth angle ($±1°$) for $40°$ ($±1°$) incidence angle and a 7 m/s ($±2$ m/s) wind speed. The top and bottom panels are respectively for VV and HH polarization. The vertical bars indicate the spread of the Doppler measurements. As observed, the spread is significant. It can be explained by several factors such as the shift in time between ECMWF outputs and ASAR acquisition, errors in the wind from the model, other geophysical phenomena such as rain (it impacts the roughness and the local wind speed at a resolution not resolved by NWP models), the errors in the Doppler estimates and the nongeophysical corrections applied to the Doppler centroid to get the geophysical Doppler. The areas where strong currents occur have been filtered out.

In the absence of an underlying sea surface current, the Doppler shift induced by the near surface wind is interpreted as the mean line-of-sight of sight velocity of the radar detected scatter elements [7]. Considering the Bragg mechanism, the velocity of these roughness elements is fixed and related to their phase velocity. However, as tilted by longer waves, the NRCS varies along these wave profiles, leading to correlation
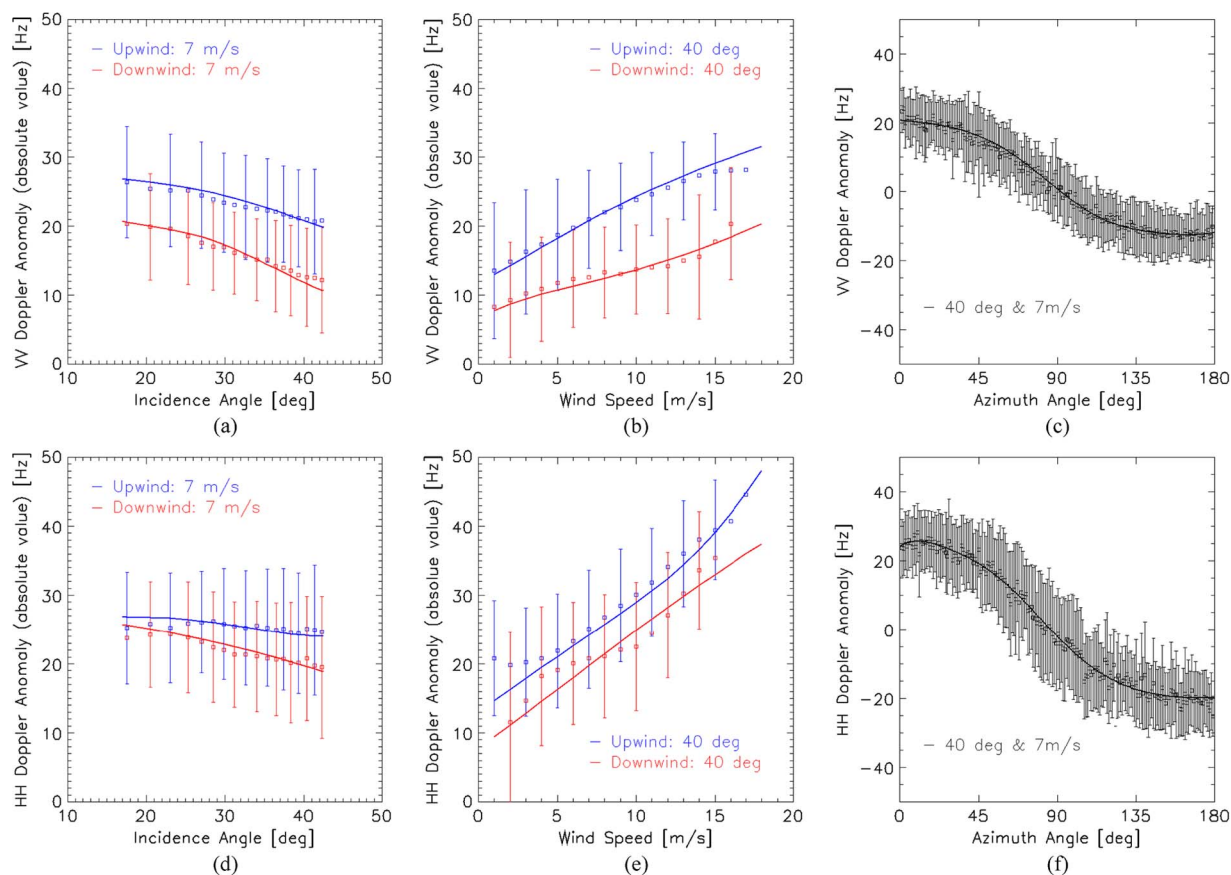
Fig. 1. CDOP and Doppler anomaly with respect to radar configuration and 10 m height wind properties. Top (respectively bottom) panel is for VV (respectively HH) polarization. (a) and (d) Doppler anomaly as a function of incidence angle for 7 m/s wind speed in upwind (blue) and downwind (red) configurations. (b) and (e) Doppler anomaly as a function of wind speed for upwind (blue) and downwind (red) at 40° incidence angle. (c) and (f) Doppler anomaly as a function of wind direction (relative to the antenna look direction) for a 7 m/s wind speed at 40° incidence angle.

with horizontal and vertical orbital velocities. Consequently, the Doppler shift is first strongly dependent upon the strength of the tilt modulation. Thus, for a given incidence angle and wind direction, the Doppler shift increases with increasing wind speed [see Fig. 1(b) and (e)]. The contribution of the tilting surface waves relative to the Bragg waves contribution is expected to depend also on the incidence angle. Since the weight of the smallest and slowest waves (Bragg) contributing to the backscattering increases with incidence, the Doppler shift decreases when incidence increases [see Fig. 1(a) and (d)]. For a given incidence angle and wind speed, the Doppler is also strongly dependent on the wind direction relative to the antenna look direction. The Doppler shift reaches a maximum (minimum) in upwind (downwind) configuration and becomes zero when the wind is blowing in the azimuth direction [see Fig. 1(c) and (f)]. The Doppler shift is thus sensitive to the wind direction, which is particularly interesting for SAR wind retrieval, as reliable wind direction estimates are rare. Doppler shifts obtained at HH polarization are always larger than at VV. This is due to the relative weaker contribution of Bragg waves (compared to the larger and faster scales) in HH than in VV polarization [9], [14]. To interpret upwind/downwind Doppler shift differences, both hydrodynamical modulation and nature of the scattering mechanism can be invoked, as well as possible skewness asymmetries for the tilting waves. To leading order, these combined effects all contribute to increase the

mean NRCS and Doppler shift in the upwind situation. As also previously discussed by [15], the relative weight of the Bragg scattering mechanism is also measurably larger for downwind looking configuration, and the Doppler shift will then decrease accordingly.

From the database of colocated ASAR Doppler measurements and ECMWF winds, we then developed an empirical function which relates the Doppler shift at C-band to wind and radar configuration

$$f^{\mathrm{DA}} = \mathrm{CDOP}(\phi, u_{10}, \theta, \mathrm{pol}). \qquad (1)$$

The function, called CDOP, is developed using a three-layer neural network and is based on the method outlined by [17]. The full expression of the GMF and its coefficients are given in the Appendix. Doppler shift from CDOP is plotted on Fig. 1 as black lines and fits the data. To validate CDOP on an independent data set, we collocated wind measurements at 10 m height from the ASCAT scatterometer (ASCAT 12.5-km wind product, [16]) with C-band ASAR Doppler anomalies. We built a match-up database between wind speed and direction from ASCAT, collocated with incidence angle and Doppler measurements from ASAR leading to 576830 and 113462 colocations for VV and HH polarizations, respectively. For HH the RMS and mean difference between simulated and measured Doppler
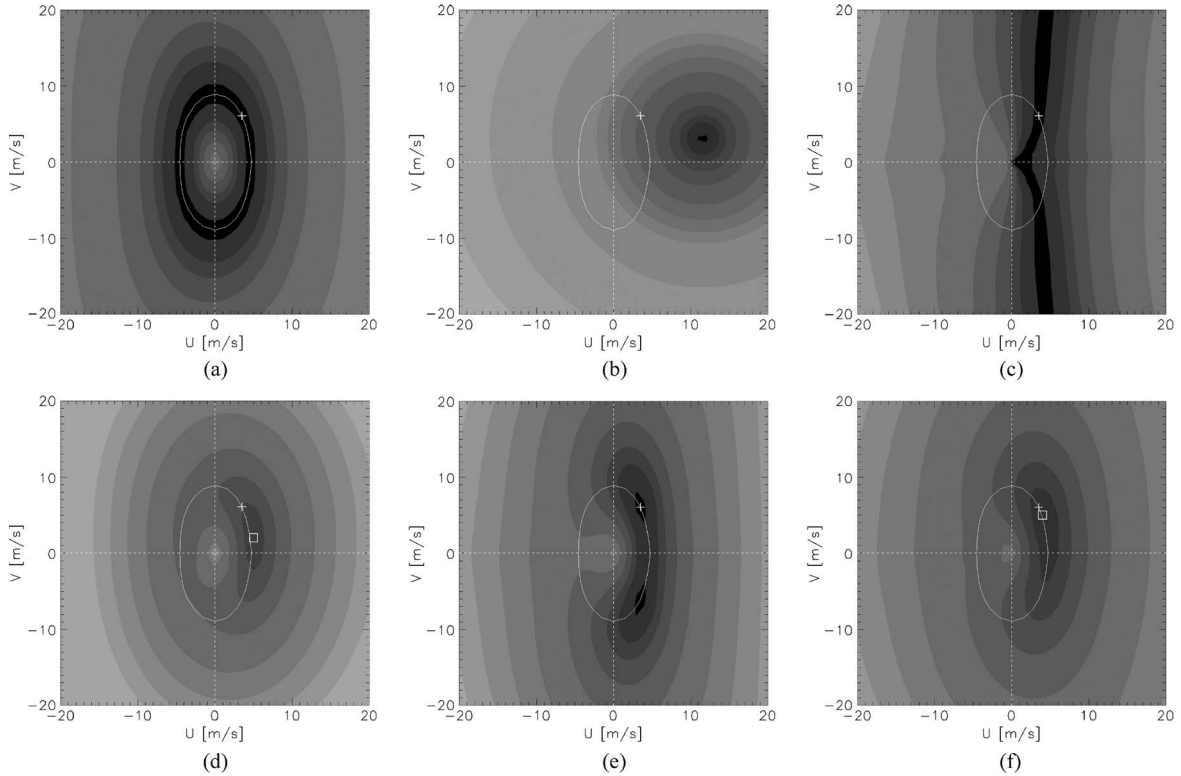
Fig. 2.   Illustration of the terms of the cost function of (2) with respect to wind zonal (u) and meridional (v) components. We consider a hypothetical case with true wind of 7 m/s blowing toward the radar 60° off the radar look direction, and an incidence angle of 30°. We choose a model (*a priori*) wind of 12 m/s and direction of 30°. Darker shading indicates lower value of the cost function terms, and higher likelihood of the solution for the wind, (a) NRCS term. (b) *a priori* (model) term (c) Doppler term. (d) NRCS and NWP combined. (e) NRCS and Doppler combined. (f) NRCS, Doppler, and model combined. A white cross indicates the true wind situation, whereas the white squares indicate the local minima for cost function. The white ellipse is the space of solution found using (5).

are, respectively, 6.5 Hz and 1.8 Hz. For VV, we found 5.23 Hz and 1.58 Hz, respectively.

III. WIND INVERSION

A. Theoretical Background

Reference [6] first proposed a methodology combining SAR information with *a priori* information, taking into account that all sources of information, both observations and models, may contain errors. Here, this method is extended to add the information contained in the Doppler shift. Simultaneous observations of NRCS (σ^0) and Doppler (f^{DA}) are assumed to be independent and related to the wind vector $\mathbf{u}$ by the CMOD and CDOP transfer functions, respectively. Following [6], we assume Gaussian errors for observations, GMFs, and the model information. This leads to a minimization problem for the determination of the maximum probability to get a wind vector given $\{\sigma^0, f^{DA}\}$

$$J(\mathbf{u}) = \underbrace{\left(\frac{\sigma^0 - \mathrm{CMOD}(\mathbf{u})}{\Delta\sigma^0}\right)^2}_{\text{NRCS term}} + \underbrace{\left(\frac{f^{DA} - \mathrm{CDOP}(\mathbf{u})}{\Delta f^{DA}}\right)^2}_{\text{Doppler term}} + \underbrace{\left(\frac{\mathbf{u} - \mathbf{u}_B}{\Delta\mathbf{u}}\right)^2}_{\substack{A\ priori \\ \text{model term}}} \quad (2)$$

where, $\mathbf{u}_B$ is the *a priori* wind vector. $\Delta\sigma^0$, Δf^{DA}, and $\Delta\mathbf{u}$ are the Gaussian standard deviation errors for the NRCS, the Doppler shift, and the model wind vector. Errors in the GMF CMOD or CDOP and NWP prior errors are expected to be spatially correlated, but not accounted for in this inversion scheme that is applied wind cell by wind cell. The zonal and meridional components of the wind vector $\mathbf{u} = \{u, v\}$ are assumed to be independent, and the last term in (2) can be written as

$$\left(\frac{\mathbf{u} - \mathbf{u}_B}{\Delta\mathbf{u}}\right)^2 = \left(\frac{u - u_B}{\Delta u}\right)^2 + \left(\frac{v - v_B}{\Delta v}\right)^2. \quad (3)$$

To illustrate and discuss the contribution of each term of the cost function, we consider a hypothetical case with "true" wind speed of 7 m/s and direction 60° with respect to the antenna look direction. We assume that the NWP model gives incorrect wind field information (speed: 12 m/s, direction: 15°) as might be expected in complex meteorological situations with distinct wind fronts. The terms of the cost function are computed and shown in Fig. 2 for an incidence angle of 30° and wind components $\{u, v\}$ ranging from −20 to 20 m/s. For the errors, we chose $\Delta\sigma^0 = 0.5$ dB [8], $\Delta f^{DA} = 5$ Hz [11] and $\Delta\mathbf{u} = \{\sqrt{3}; \sqrt{3}\}$ m/s [6].

Darker shading means lower values of the cost function, i.e., a more likely wind vector. The white cross in Fig. 2 indicates the "true wind" situation. "True NRCS and Doppler" are calculated

using CMOD and CDOP, respectively. The white squares indicate the result obtained after minimization of the cost function. Fig. 2(a)–(c) illustrates the contribution to the cost function from the NRCS, model, and Doppler terms, respectively. When only the NRCS is used to compute the cost function, there are several minima (elliptic shape) corresponding to an underconstrained problem. The addition of the model term [Fig. 2(b) and (d)] accounts for both wind speed and direction and their associated errors. When the *a priori* information departs too much from the real wind situation, the Bayesian approach cannot compensate the error. As shown in Fig. 2(c), the use of Doppler shift alone would also lead to an underconstrained problem. On the other hand, as shown in Fig. 2(e), the NRCS and Doppler cost functions have distinct different shapes which complement each other. In this case, the number of possible solutions is dramatically reduced. Yet, ambiguities remain, and *a priori* information is still needed in our inversion scheme when a unique solution is required. The total cost function [(2)] is shown on Fig. 2(f). All in all, the comparison of results with [Fig. 2(d)] and without [Fig. 2(d)] the Doppler term in the cost function illustrates how the Doppler shift helps to get better winds.

As noticed by [18], the minimization can be reformulated if the NRCS is assumed free of noise and if an inverse GMF is used to relate radar configuration, NRCS, and wind direction (with respect to the antenna look angle) to the wind speed

$$u_{10} = \text{GMF}^{-1}(\theta, \phi, \sigma^0, \text{pol})\big|_{\phi \in [0, 360°]}. \tag{4}$$

This inverse GMF enables to determine the possible solutions $\{u_{10}, \phi\}$ (or $\{u, v\}$) for a given radar configuration and NRCS. Thus, combining (2) and (4), the cost function becomes

$$J(\mathbf{u}) = \left(\frac{f^{DA} - \text{CDOP}(\mathbf{u})}{\Delta f^{DA}}\right)^2$$
$$+ \left(\frac{\mathbf{u} - \mathbf{u}_B}{\Delta \mathbf{u}}\right)^2\Bigg|_{\{u_{10} = \text{GMF}^{-1}(\theta, \phi, \sigma^0, \text{pol}), \phi\}}. \tag{5}$$

The space of solutions obtained with (4) in the context of the previous simulation exercise is presented by the white ellipse on Fig. 2.

Such kind of minimization performed wind cell by wind cell in the SAR image is a local inversion. It does not take account of spatially correlated errors, e.g., sea state errors in the GMF and NWP prior errors are expected to be spatially correlated, but not accounted for.

B. Application and Validation

We have selected two cases of complex meteorological situations to illustrate the wind signature of the Doppler shift, and the performance of the method outlined in Section III. The NRCS and the Doppler shift in VV polarization from Envisat ASAR are shown in Fig. 3 together with ASCAT scatterometer winds for a case with an atmospheric front (upper panels) and for a low pressure system (lower panels). The NRCS wind dependency is more driven by the wind speed than the direction,

whereas strong gradients of NRCS are generally associated with rapid changes of the wind direction on short spatial scales. Concerning the Doppler shift, in agreement with Section II, there is expectedly a strong dependency on the wind direction relative to the antenna look direction. For wind blowing along the azimuth direction, the Doppler signal due to wind vanishes and becomes positive (negative) for wind blowing toward (away from) the radar. In addition, for a given direction, the Doppler shift increases with wind speed. For an easier geophysical interpretation, the Doppler shifts are converted to surface radial velocity by the relation

$$V_{\text{rad}} = -\frac{\lambda_0 f^{DA}}{2 \sin \theta}$$

where λ_0 is the radar wavelength and θ is the incidence angle.

In the case of the atmospheric front [Fig. 3(a)–(c)], ASCAT indicates that north of the front, the wind blows from north—northeast and turns abruptly to become north-westerly oriented. Comparing with ASAR NRCS, it can be observed that no matter the wind direction, the NRCS increases with increasing wind speed. Near the front, strong ASAR NRCS gradients, ASCAT wind direction changes and radial velocities sign switches are correlated. Thus, the combination of NRCS and Doppler, can give a qualitative indication about the wind field structure for a given scene.

In the case of the low pressure system [Fig. 3(d)–(f)], ASCAT wind exhibits a clear circular pattern of the wind due to the low pressure system. The changes of sign for the radial velocities are consistent with this circular pattern. The sign is positive south of the low pressure center where the circulation of the flow is easterly, and negative to the north, where the flow is westerly. The radial velocities are also in very good agreement with ASCAT wind field.

For both these cases, we compared three different schemes: 1) scatterometry approach where wind is calculated with the CMOD function [12] and the wind direction is given by a model; 2) the Bayesian scheme where only NRCS and model information are used; and 3) the Bayesian scheme combining Doppler, NRCS and model. Results by using the cost function of (5) are presented in Fig. 4. Comparison with the ASCAT wind fields clearly demonstrates the benefit of using the Doppler with NRCS for wind inversion. When the Doppler shift is included, the wind pattern as obtained with ASAR compares very well with ASCAT results. For the low pressure system, the circular wind pattern is well captured by SAR when Doppler is used [see Fig. 4(f)]. For the case with the atmospheric front, when Doppler is used, the location of the abrupt shift of wind direction is located where there is a strong gradient of NRCS, in agreement with the ASCAT wind [see Fig. 3(c)].

For a quantitative validation, we have colocated 103 SAR images with wind measured by NDBC buoy number 42056 in the Caribbean Sea without any particular selection of meteorological situations. These cases do not correspond to any particular complex meteorological situations, and the model is not expected to be dramatically wrong. The statistics of the results obtained using the Bayesian scheme with and without
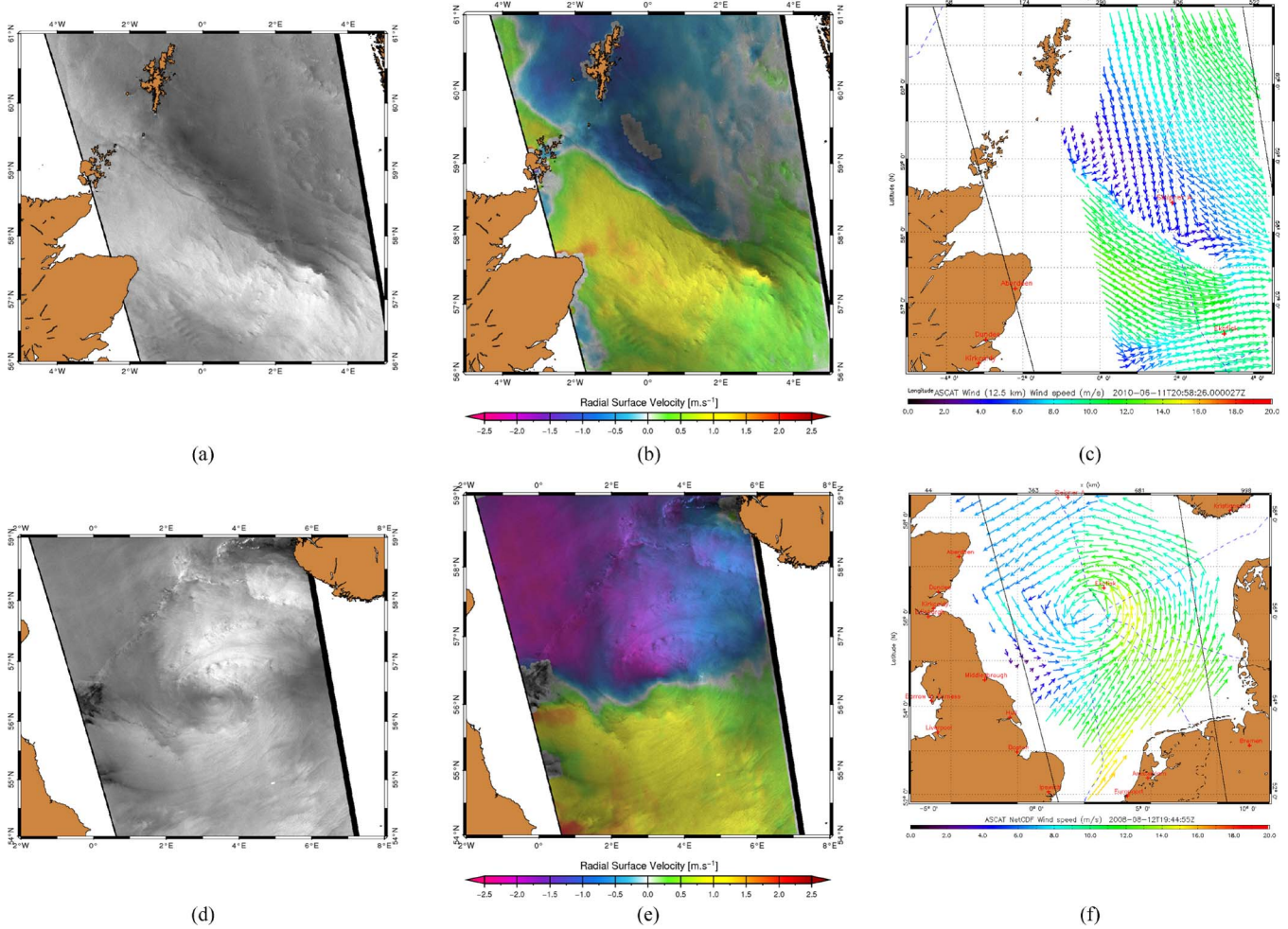
Fig. 3.   Two examples of wind signatures in the NRCS (left) and Doppler velocity signal (center) as measured by ASAR and corresponding wind field retrieved with ASCAT (right). The upper panels show a case with an atmospheric front on 11 June 2010 at 21:27:32 UTC, and the lower panels show a case with a low pressure system on 12 August 2008 at 21:20:58 UTC. The sign convention for the radial velocity is such that when radial velocity is positive (respectively negative) wind is blowing from the west (respectively east).

the Doppler are shown in Table I. The wind direction is much more accurate for the scheme including the Doppler shift, with a RMS of 14°, compared to 30° for the same scheme without the Doppler information. This improvement in the wind direction RMS is due to the few cases where the *a priori* information and the *in situ* measurement are strongly inconsistent. For the wind speed, we find in fact a slightly decreased performance when Doppler shift is included. It is likely due to the high uncertainty of the Doppler centroid anomaly, as it is still to be considered as an experimental derived quantity in the Envisat ASAR ground segment. In particular, when the *a priori* wind information and the NRCS are very consistent, the use of Doppler anomaly can add noise to lower the performance the inversion scheme (Table II).

IV. CONCLUSION

Hitherto the investigations of the Doppler shift signals have mostly been conducted in areas with strong surface currents, such as in the Agulhas Current, to derive and analyze estimates of the surface current [9]. However, as demonstrated by [7]

the Doppler shift anomaly results from a mixture of sea state displacements from the wind, waves, and currents.

This study shows that the Doppler anomaly as measured by SAR at C-band is indeed wind dependent with respect to polarization, incidence angle, and antenna look direction. This dependency is found to be complementary to the NRCS. Using a Bayesian scheme, we demonstrate how these two radar quantities, i.e., NRCS and Doppler anomaly, could be advantageously used to increase the weight of the SAR data in the SAR wind inversion schemes. In particular, it is found that the high sensitivity of the Doppler to the wind direction is useful to retrieve more realistic wind patterns in cases of complex and rapidly changing meteorological situations. Thus, for coastal wind regimes and extreme events such as hurricanes, typhoons, and polar lows where the SAR images may be colocated with incorrect *a priori* wind field information (particularly the wind direction) the incorporation of the Doppler shift will provide highly valuable information.

Today, the Doppler shift is not provided as a geophysical product and is not routinely used for geophysical inversion by the scientific community. Accordingly, the precision requirements, which are a few Hertz for sea surface current estimation
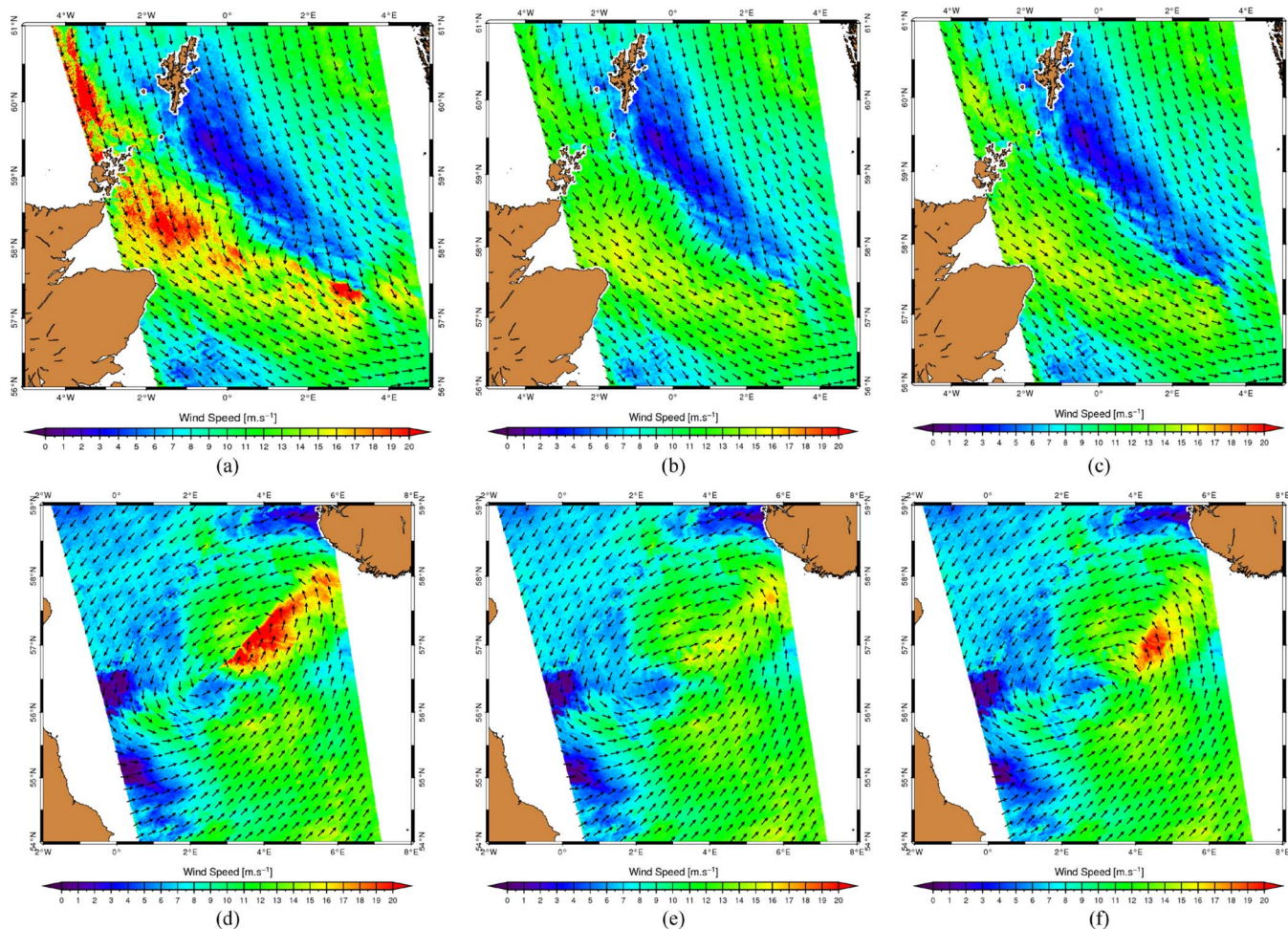
Fig. 4. (Top panel) Case of an atmospheric front on 11 June 2010 at 21:27:32 UTC. (a) Scatterometry approach, where the wind direction is given by the *a priori* information. (b) Bayesian scheme without Doppler shift, (c) Bayesian scheme including Doppler. (Bottom panel) The same for the case of a low pressure system on 11 June 2010 at 21:27:32 UTC.

TABLE I
STATISTIC OF VALIDATION EXERCISE PERFORMED
AGAINST *IN-SITU* MEASUREMENTS

		Without Doppler	With Doppler
Wind direction	Bias [deg]	-1.52	-1.79
	RMS [deg]	30.0	14.1
Wind speed	Bias [m/s]	-0.63	-0.65
	RMS [m/s]	0.97	1.20

or wind estimation, are not yet achieved. Additional correction steps must thus be performed. In particular, antenna characteristics have to be more accurately known. Yet, the results found in this study are very encouraging. In particular, for future SAR missions such as Sentinel-1, the Doppler anomaly will be a standard component of the L2 ocean product. The method will then benefit of more accurate Doppler anomalies and a new improved version of CDOP could be developed. In the future, the Bayesian scheme could further be improved by using a nonlocal inversion scheme and a better description of the error structures.

New more accurate radar quantities are then foreseen to provide improved information for both wind field and surface current inversions. Ideally, next refined step could thus be a more consistent synergetic approach where the NRCS and the Doppler shift information would be combined to derive improved estimates of both the near surface wind field and the sea surface currents (using *a priori* routine atmosphere and ocean circulation model first guess). A complementary Doppler and NRCS capability may be interesting for future scatterometer systems. Indeed, the multi-azimuth angular dependence associated with NRCS and Doppler measurements would then allow better constraining the inversion problems.

APPENDIX

Doppler shift due to sea surface wind can be written as

$$\Delta f_{pp} = \alpha_{pp} F \left[X(\theta, \phi, u_{10}, pp) \right] + \beta_{pp}$$

where θ is the incidence angle in degree, ϕ the wind direction with respect to the antenna look angle in degrees (where 0 (respectively, 180°) means wind blows toward (respectively, against) the antenna. Thus, 90° and 270° mean wind blow in direction perpendicular to the antenna look direction.), u_{10} the

TABLE II
SET OF $\omega_{i,j}$ COEFFICIENTS FOR HH AND VV POLARIZATIONS

$\omega_{i,j}^{HH}$	j=0	j=1	j=2	j=3
i=1	1.30653883096	-9.07176856257	-0.973599180956	-2.61087309812
i=2	-2.77086154074	-0.594867645776	0.586523978839	-0.246776181361
i=3	10.6792861882	16.9815377306	12.9439063319	17.9261562541
i=4	-4.04296669064	-9.20238868219	6.20098098757	0.595882115891
i=5	-0.172201666743	-4.12397246171	0.301856868548	-0.993509213443
i=6	20.4895916824	8.57886720397	17.643307099	15.0224985357
i=7	28.2856865516	-15.1439734434	20.6983195925	13.1833641617
i=8	-3.60143441597	-9.9811757434	5.79854593024	0.656338134446
i=9	-3.53935574111	11.9861607453	-5.67640781126	0.122736690257
i=10	-2.11695768022	-16.0530462	5.95289490539	0.691577162612
i=11	-2.57805898849	7.93435940581	0.151056851685	1.2664066483

$\omega_{i,j}^{VV}$	j=0	j=1	j=2	j=3
i=1	14.5077150927	1.27887019276	22.2237414308	19.7873046673
i=2	-11.4312028555	16.4242081101	-3.63395681095	2.910815875
i=3	1.28692747109	0.325018607578	0.403986575614	1.03269004609
i=4	-1.19498666071	0.969975702316	4.47461213024	3.17100261168
i=5	1.778908726	-0.016265075646	-6.91334859293	-3.80611082432
i=6	11.8880215573	-13.4031862615	-1.64290475596	4.09854466913
i=7	1.70176062351	-6.04613303002	-1.30503436654	0.484338480824
i=8	24.7941267067	23.2186869807	15.993470129	-11.1000239122
i=9	-8.18756617111	6.13874672206	0.801977535733	-0.577883159569
i=10	1.32555779345	-4.42736737765	-0.5009830671	0.61008842868
i=11	-9.06560116738	8.94943709074	1.31351068862	-1.94654022702

wind speed and pp denotes the polarization. α^{pp} and β^{pp} are two coefficients depending on polarization

$$\alpha^{vv} = 111.528184073 \quad \text{and} \quad \beta^{vv} = -52.2644487109$$

$$\alpha^{hh} = 136.216953823 \quad \text{and} \quad \beta^{hh} = -66.9554922921$$

and $F[x]$ is defined as

$$F(x) = \frac{1}{1 + e^{-x}}$$

$$X(\theta, \phi, u_{10}, pp) = \gamma_0^{pp} + \sum_{i=1}^{11} \gamma_i^{pp} F\left[\Gamma_i^{pp}(\theta, \tilde{\phi}, u_{10})\right]$$

where

$$\Gamma_i^{pp}(\theta, \tilde{\phi}, u_{10}) = \omega_{i,0}^{pp} + \omega_{i,1}^{pp} V_1(\tilde{\phi}) + \omega_{i,2}^{pp} V_3(u_{10}) + \omega_{i,3}^{pp} V_2(\theta)$$

$$V^{pp} = \begin{pmatrix} V_1^{pp} \\ V_2^{pp} \\ V_3^{pp} \end{pmatrix} = \begin{pmatrix} \tilde{\phi} \cdot \lambda_{20}^{pp} + \lambda_{21}^{pp} \\ \theta \cdot \lambda_{00}^{pp} + \lambda_{01}^{pp} \\ u_{10} \cdot \lambda_{10}^{pp} + \lambda_{11}^{pp} \end{pmatrix}$$

$$\tilde{\phi} = \begin{cases} 360° - \phi, & \text{if } \phi < 180° \\ \phi, & \text{otherwise.} \end{cases}$$

The set of coefficients ω for each polarization is given in Table II.

ACKNOWLEDGMENT

The authors would like to thank the European Space Agency (ESA) and in particular Betlem Rosich that helped modify ENVISAT ASAR Wide swath products to include Doppler centroid grids. This work was supported by ESA under

REFERENCES

[1] F. M. Monaldo and V. Kerbaol, "The SAR measurement of ocean surface wids: An overview," in *Proc. 2nd Workshop Coastal Marine Appl. SAR, 8–12 September 2003*, Svalbard, Norway, Jun. 2004, ESA SP-565.
[2] A. Stoffelen and D. Anderson, "Scatterometer data interpretation: Estimation and validation of the transfer function CMOD4," *J. Geophys. Res.*, vol. 102, no. C3, pp. 5767–5780, 1997.
[3] F. M. Monaldo, D. R. Thompson, W. G. Pichel, and P. Clemente-Colon, "A systematic comparison of QuikSCAT and SAR ocean surface wind speeds," *IEEE Trans. Geosci. Remote Sens.*, vol. 42, no. 2, pp. 283–291, Feb. 2004.
[4] W. Koch, "Directional analysis of SAR images aiming at wind direction," *IEEE Trans. Geosci. Remote Sens.*, vol. 42, no. 4, pp. 702–710, Apr. 2004.
[5] C. C. Wackerman, C. L. Rufenach, R. A. Shuchman, J. A. Johannessen, and K. L. Davidson, "Wind vector retrieval using ERS-1 synthetic aperture radar imagery," *IEEE Trans. Geosci. Remote Sens.*, vol. 34, no. 6, pp. 1343–1352, Nov. 1996.
[6] M. Portabella, A. Stoffelen, and J. A. Johannessen, "Toward an optimal inversion method for SAR wind retrieval," *J. Geophys. Res.*, vol. 107, p. 8, 2002, doi:10.1029/2001JC000925.
[7] B. Chapron, F. Collard, and F. Ardhuin, "Direct measurements of ocean surface velocity from space: Interpretation and validation," *J. Geophys. Res.*, vol. 110, p. C07008, Jul. 2005.
[8] *ASAR Product Handbook*, 2007, issue 2.2.
[9] J. A. Johannessen, B. Chapron, F. Collard, V. Kudryavtsev, A. Mouche, D. Akimov, and K.-F. Dagestad, "Direct ocean surface velocity measurements from space: Improved quantitative interpretation of Envisat ASAR observations," *Geophys. Res. Lett.*, vol. 35, p. L22608, Nov. 2008, doi:10.1029/2008GL035709.
[10] M. J. Rouault, A. Mouche, F. Collard, J. A. Johannessen, and B. Chapron, "Mapping the Agulhas current from space: An assessment of ASAR surface current velocities," *J. Geophys. Res.*, vol. 115, p. C10026, Oct. 2010, doi:10.1029/2009JC006050.

[11] M. W. Hansen, F. Collard, K. Dagestad, J. A. Johannessen, P. Fabry, and B. Chapron, "Retrieval of sea surface range velocities from Envisat ASAR Doppler centroid measurements," *IEEE Trans. Geosci. Remote Sens.*, vol. 49, no. 10, pp. 3582–3592, 2011, doi:10.1109/TGRS.2011.2153864.

[12] Y. Quilfen, B. Chapron, T. Elfouhaily, K. Katsaros, and J. Tournadre, "Observation of tropical cyclones by high-resolution scatterometry," *J. Geophys. Res.*, vol. 103, no. C4, pp. 7767–7786, 1998, doi:10.1029/97JC01911.

[13] H. Hersbach, A. Stoffelen, and S. de Haan, "An improved C-band scatterometer ocean geophysical model function: CMOD5," *J. Geophys. Res.*, vol. 112, p. C03006, Mar. 2007, doi:10.1029/2006JC003743.

[14] A. Mouche, B. Chapron, N. Reul, and F. Collard, "Predicted Doppler shifts induced by ocean surface displacements using asymptotic electromagnetic wave scattering theories," *Waves Random Complex Media*, vol. 18, no. 1, pp. 185–196, Feb. 2008.

[15] B. Chapron, V. Kerbaol, and D. Vandemark, "A note on relationship between sea-surface roughness and microwave polarimetric backscatter measurements: Results from POLRA-96," in *Proc. POLRAD'96 Int. ESA Workshop, ESA WPP-135, ESTEC*, Noordwijk, The Netherlands, Apr. 29, 1997.

[16] *ASCAT 12.5 km Wind Product User Manual v 1.8*, OSI-SAF Project Team, 2010.

[17] F. Collard, A. Mouche, B. Chapron, C. Danilo, and J. Johannessen, "Routine high resolution observation of selected major surface currents from space," in *Proc. SEASAR Symp., SP-656, ESA, ESA-ESRIN*, Frascati, Italy, 2008.

[18] V. Kerbaol, "Improved Bayesian wind vector retrieval scheme using ENVISAT ASAR data: Principles and validation results," in *Proc. ENVISAT Symp.*, Montreux, Switzerland, Apr. 23–27, 2007.

Alexis A. Mouche received the Master degree in physics for remote sensing from the University of Pierre et Marie Curie, Paris, France, in 2002. From 2002 to 2005, he worked as a Ph.D. student at CETP/IPSL/CNRS (National Research Center) and received the Ph.D. degree in physics with a focus on ocean remote sensing in 2005.

Since January 2006, he has been working on approximate scattering wave theories from random ocean surface in the Spatial Oceanography group at IFREMER, Brest, France. This postdoctoral position was Granted by CNES (French Space Agency). He joined BOOST Technologies in 2008 and works now in the R&D Department at the Radar Applications Division of CLS, Plouzané, France.

Fabrice Collard received the M.S. degree from the Ecole Centrale de Lyon, Ecully, France, in 1996, where he studied off-shore engineering and the Ph.D. degree in oceanography and meteorology from Paris 6 University, Paris, France, in 2000.

His thesis was dedicated to the 3-D aspect of wind-wave field. He spent two years working on HF radars as a postdoctoral research associate at RSMAS, Miami. He is currently Head of the R&D Department at the Radar Applications Division of CLS, Plouzané, France, working on the development and validation of surface wind, wave, and current retrieval from synthetic aperture radar.

Bertrand Chapron was born in Paris, France, in 1962. He received the B.Eng. degree from the Institut National Polytechnique de Grenoble, Grenoble, France, in 1984 and the Doctorat National (Ph.D.) degree in fluid mechanics from the University of Aix-Marseille II, Marseille, France, in 1988.

He spent three years as a Post-Doctoral Research Associate at the NASA/GSFC/Wallops Flight Facility, Wallops Island, VA. He has experience in applied mathematics, physical oceanography, electromagnetic waves theory, and its application to ocean remote sensing. He is currently responsible for the Oceanography from Space Laboratory, IFREMER, Plouzané, France.

Knut-Frode Dagestad received the Cand. Scient. and Dr. Scient. degrees from University of Bergen, Bergen, Norway, in 2000 and 2005, respectively.

The thesis work was performed at the Geophysical Institute, in the field of atmospheric radiative transfer with application to solar energy. Since 2005, he has been working with remote sensing at the Nansen Environmental and Remote Sensing Center, Bergen. The main research interest is retrieval of wind, waves, and currents from remote sensing data, with focus on synthetic aperture radar.

Gilles Guitton received the M.Sc. degree from ENST-Bretagne, Brest, France, in 2007, within spatial oceanography and ocean monitoring, where he is currently working toward the Ph.D. degree on hurricanes.

During his M.Sc. degree study, he visited Norut, Tromsø, Norway, from April 2006 to October 2006, as a Trainee, where he worked with an EM scattering model for the ocean surface.

Johnny A. Johannessen received the Dr. Philos. degree from the University of Bergen, Bergen, Norway, in 1997.

He is Vice Director at the Nansen Environmental and Remote Sensing Center, Bergen. His experience in satellite remote sensing in oceanography and sea ice research is broad and comprehensive. In particular, he has focused on the use of synthetic aperture radarimaging capabilities to advance the understanding of mesoscale processes along the marginal ice zone and in vicinity of ocean fronts and eddies. In the last 10 years, he has also been involved in development and implementation of operational oceanography and marine forecasting both at national and international level.

Vincent Kerbaol graduated from the Ecole Nationale Supérieure des Télécommunications de Bretagne, Bretagne, France, in 1992 with emphasis in image processing. He received the Ph.D. degree in signal/image processing and remote sensing from the University of Rennes 1, Rennes, France, in 1997.

He is Head of the Radar Applications Divisions at CLS, Plouzané, France. After doing his civil service in Tromsoe, Norway, he worked as a Ph.D. student on ocean synthetic aperture radar (SAR) Images at the Oceanography from Space laboratory at IFREMER, Brest France. He stayed at IFREMER up to February 1999, as a postdoc Granted by CNES (French space agency), mainly working on altimetry. In March 1999, He joined the ENST Bretagne in the Départment Signal and Communications as an Assistant Professor. His works mainly include sea state retrieval, from SAR imagery and altimetry, radar technology, and signal/image processing.

Morten Wergeland Hansen received the Cand. Scient. degree in astrophysics from the University of Oslo, Oslo, Norway, in 2004, with a thesis on the orbits of Jupiter's Galilean satellites and the M.Sc. degree in space studies from the International Space University, Strasbourg, France, in 2006, with a thesis on the validation of level-2 products from the atmospheric instruments aboard Envisat.

He has been with the Nansen Environmental and Remote Sensing Center, Bergen, Norway, since 2007 as a Research Assistant and later as a Ph.D. candidate with focus on the development and utilization of the Doppler velocity product from Envisat ASAR.